IEEE Access
Multidisciplinary | Rapid Review | Open Access Journal

Received December 29, 2019, accepted February 8, 2020, date of publication February 14, 2020, date of current version February 26, 2020.

Digital Object Identifier 10.1109/ACCESS.2020.2974036

Modelling and Control of Modular DC-Nanogrids Based on Loss-Free Resistors

REHAM HAROUN, (Member, IEEE), ABDELALI EL AROUDI, (Senior Member, IEEE), ANGEL CID-PASTOR, (Member, IEEE), ENRIC VIDAL-IDIARTE, (Member, IEEE), HUGO VALDERRAMA-BLAVI, (Member, IEEE), AND LUIS MARTINEZ-SALAMERO, (Senior Member, IEEE)

Departament de Enginyeria Electrònica, Elèctrica i Automàtica, Escola Tècnica Superior d'Enginyeria, Universitat Rovira i Virgili, 43007 Tarragona, Spain

Corresponding author: Reham Haroun (reham.haroun@urv.cat)

This work was supported in part by the Spanish Agencia Estatal de Investigacion (AEI), and in part by the Fondo Europeo de Desarrollo Regional (FEDER) under Grant DPI2015-67292-R, DPI2016-80491-R and Grant DPI2017-84572-C2-1-R (AEI/FEDER, UE).

ABSTRACT This paper proposes a modular photovoltaic (PV) dc-Nanogrid (dc-NG) architecture for residential applications. The proposed architecture is based on the Loss-Free Resistor (LFR) concept. The dc distribution bus is supplied by PV panels, ac utility and a storage battery. The storage battery is connected to the main dc bus through a dc-dc bidirectional converter (BDC). This battery has also an important role to ensure uninterruptible power supply to the critical loads and controls the power flow in the dc-NG. A mathematical model of the system is first derived and a stability analysis is carried out showing that the stability is guaranteed under certain mild conditions. Numerical simulations of a case study for two PV panels corroborate the theoretical predictions which have been finally confirmed by experimental measurements.

INDEX TERMS Loss-free resistor (LFR), dc-nanogrid (dc-NG), sliding mode control (SMC), bidirectional converter (BDC).

I. INTRODUCTION

Future power grids will no longer be dominated by coal-fired power stations. The production of electrical energy will also be based on distributed generation sources such as solar photovoltaic (PV) arrays, wind turbines and batteries forming nano and micro grids [1], [2]. In particular, solar photovoltaic (PV) technology is considered as one of the most environmentally-friendly energy sources since it generates electricity with almost zero emissions while requiring very low maintenance efforts. Therefore, PV panels are the most important renewable energy sources that can meet power requirements of residential applications without jeopardizing the aesthetics of the building [3], [4]. This explains the increasing demand of PV arrays installation in homes and small companies in both grid-connected and in stand-alone operation modes.

DC nanogrids (dc-NGs) are gaining interest in different places such as remote areas, recharging stations for electric vehicles (EVs), data centers and residential areas [5]. Besides, they can be interconnected to form a microgrid for a relatively large geographical region offering several advantages such as higher efficiency, reliability and modularity [1], [6]–[8].

When dc-NGs are supplied by Renewable Energy Sources (RES), they are affected by frequent and relevant energy fluctuations, which can be only mitigated by using energy storage systems to ensure uninterruptible power supply to the critical loads and to maintain the power balance in the dc-NGs [9]. Batteries are the most common and economical storage devices in medium power-range. A dc-dc converter is always required to allow energy exchange between the battery and the rest of the system. These kind of converters must have a bidirectional power flow capability with flexible control in all operating modes [10], [11].

Many techniques have been used to control bidirectional converters. As an example, in [12], [13], several control methods such as Passivity-Based Control, Immersion & Invariance and Sliding Mode Control (SMC) have been applied to a BDC loaded by a Constant Power Load (CPL). In [14], a BDC under a hysteretic controller for a battery energy storage system has been analyzed.

The associate editor coordinating the review of this manuscript and approving it for publication was Ali Zemouche.

Many research efforts have been devoted to control and stability analysis of micro and NG systems [15]–[21]. For instance, a hierarchical control system and an adaptive droop control has been introduced in [15], [16] for dc microgrids, while in [17], a simple droop control approach for autonomous power management in low voltage dc microgrids based on a master-slave concept has been presented. The distributed energy resources control and operation in a grid-connected off-grid dc microgrid have been studied in [18]. Moreover, in [19], a current controlled approach has been utilized for controlling the active power flow and the power factor of a bidirectional converter interfacing ac and dc microgrids. The stability analysis of a dc-NG has been studied using Nyquist test [20]. A frequency output impedance matrix model has been proposed to describe the output terminal frequency characteristics of a dc-dc converter in a NG around its switching frequency range [21]. Most of the research about the control and stability analysis of NGs consider the analysis of a single or two converters while ignoring the rest of the NG and the possible interactions between its different subsystems. This is mainly because of the difficulty of the analysis of the whole nanogrid under the above mentioned control approaches. Therefore, it is of primordial importance the synthesis of dc-NG without possible interactions among its composite subsystems.

The traditional description of a dc-dc switching converter as a conservative two-port circuit was due to R.D. Middlebrook [22] who established that the most appropriate model for that description was a dc transformer, i.e., a device that does not exist in nature but can be implemented electronically.

Middlebrooks paradigm was complemented some years later by the proposals of S. Singer, who introduced the notions of power gyrator [23] and Loss-Free Resistor (LFR) [24] to model the behavior of a dc-dc switching converter. The new elements were also conservative two-port circuits that completed a family of canonical elements to model any power processing circuit. The canonical elements are therefore the dc transformer, the power gyrator and the LFR, and they were categorized subsequently by S. Singer and R.W. Erickson as POPI networks [25], the acronym POPI standing for Power output-Power input, which means that the power dc at the output port equals the power dc at the input port.

These notions are not merely useful for interpreting the operation of power processing systems but they play besides an important role in the first step of designing interconnected converters. Most of the functions required in the association of converters in dc distributed power systems such as paralleling, cascading, source splitting etc. [26] can be obtained by designing dc-dc converters operating as any of the three canonical elements mentioned above. Roughly speaking, series association of ports leads to use a dc transformer approach while paralleling can be carried out using a power gyrator-based design [27].

The usefulness of an LFR-based design of a power converter has been recently revealed in the cascade connection of converters [28] and in Power Factor Correction (PFC) circuits [29], [30]. The LFR is modelled by a resistor in the input port, called emulated resistor, and a power source at the output port as shown in Fig. 1(a).

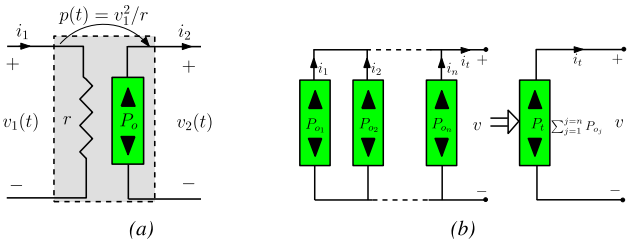

FIGURE 1. (a) Two-port model of a loss-free resistor. (b) Parallel connection of power sources.

The novelty of this work is the use of a LFR-based design for three different purposes, each of them corresponding respectively to each of the three basic blocks of the proposed nanogrid; namely, photovoltaic energy processing, ac utility connection, and bidirectional operation of the battery. The three different goals to be attained with the LFR approach are the following:

(i) Connecting in parallel the output ports of several power converters to process the energy provided by the photovoltaic generator without any circulating current. It has to be pointed out that connecting n power sources in parallel results in a new power source, which supplies the sum of the corresponding n corresponding currents and powers while supporting the same original voltage as depicted in Fig. 1(b).

(ii) Correcting the power factor in the rectifier stage.

(iii) Establishing the operation mode in the bidirectional converter, i.e., battery charging mode for a negative value of the emulated resistance of the LFR, and battery discharging mode for a positive value of that resistance.

The underlying idea in our proposal is the implementation of a nanogrid using only converters with LFR behavior in the three constitutive blocks of the system as shown in Fig. 2. The main antecedent of developing a power distributions system based on a single canonical element was reported in [31], where a dc grid was implemented using two different types of power gyrators, which were associated either in cascade or in parallel. A subsequent comparison between power gyrators and LFRs in the cascade connection of power converters in [28] revealed that LFRs exhibited a larger stability margin. Besides, converters with LFRs behavior are more versatile than converters with gyrator characteristics. Although the latter are particularly suitable for paralleling power converters [27], [32], they cannot be used in power factor correction and in bidirectional operation. the LFR approach is very important since it would simplify the construction and expansion of micro-grids powered by renewable sources in which the converters can be considered black boxes which can be aggregated without any stability problems.

In this paper, a dc-NG utilizing the LFR concept, supplying different types of loads and being supplied from different energy sources is presented. In [33], [34], a proof-of-concept of the impedance matching of a single branch

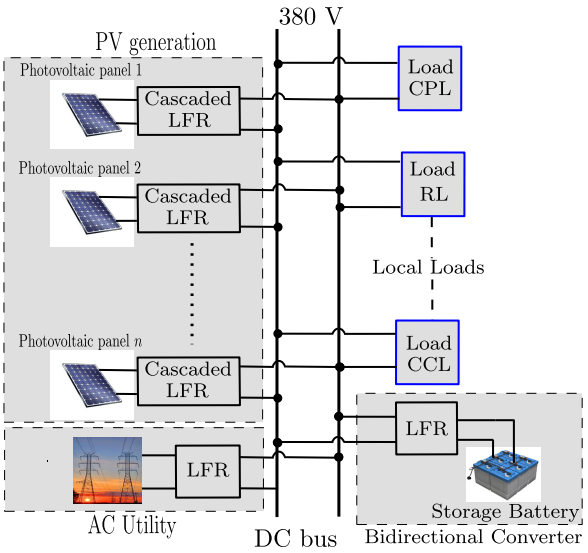

FIGURE 2. Proposed photovoltaic dc-NG based on LFR.

has been studied, and the idea is extended here to different branches constituting the modular NG. A comparison has been proved that the two cascaded boost converters is better than coupled-inductor step-up converter in terms of simplicity, stability and number of components [34], hence motivating the use of the the same cascaded converters for implementing the dc-NG. As will be shown later, the used approach facilitates the synthesis of the system, its stability analysis and its final realization. Furthermore, the same concept of LFR has been also applied to design the BDC interfacing a storage battery and the dc bus, and also, to the design of ac-dc converter to interface ac utility and the dc bus.

The rest of this paper is organized as follows. Section II presents the description of the proposed modular dc-NG which is constituted by n output-parallel-connected two-stage boost converters interfacing the PV panels to the dc bus, an ac-dc converter connected to an ac utility and finally a BDC connected to the storage battery. Section III deals with the mathematical modeling of the system and its stability analysis. Numerical simulations and experimental measurements from a case study with two branches ($n = 2$) are presented in Section IV. Finally, some concluding remarks of this study are summarized in the last section.

II. NANOGRID DESCRIPTION AND ITS MATHEMATICAL MODELLING

A. SYSTEM DESCRIPTION

Fig. 3 shows the block diagram of the proposed dc-NG. As can be seen in the same figure, different PV panels are supplying different kinds of loads through two-cascade boost converters operating as LFRs performing impedance matching [34]. The different n PV panels are connected to the regulated dc bus using n branches of two-stage boost LFR. Although decentralized storage systems can offer some benefits in terms of more reliability and less stress in the

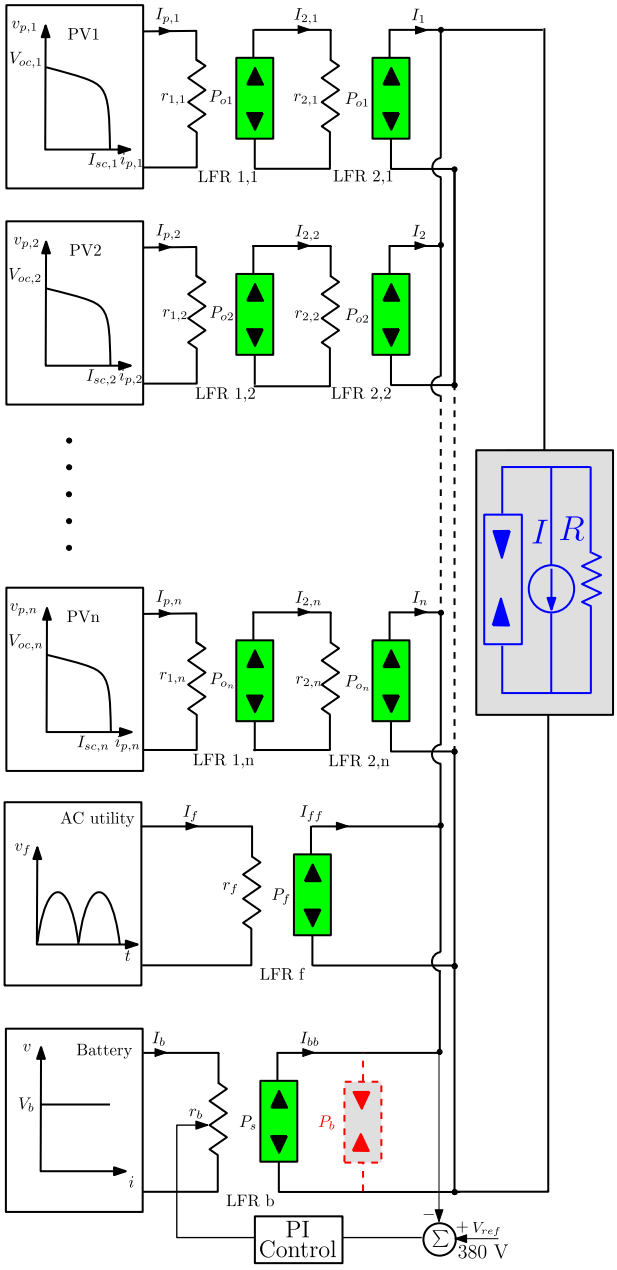

FIGURE 3. Simplified block diagram of the dc-NG under study.

devices [35], [36], our proposal uses a single battery due to the low power handled by the nanogrid. This storage battery is connected to the main 380 V dc bus using a BDC also operating as an LFR with an additional outer voltage loop for regulating the dc bus. In addition, the ac utility is connected to the same bus using an ac-dc rectifier with PFC. This PFC converter is used to connect the dc-nanogrid to the AC utility. The dc-NG can be working in stand alone if this converter is disabled. The proposed dc-NG will be loaded by different linear and nonlinear loads. The load types for dc-dc switching power converters could be mainly linear resistive or constant impedance load, linear capacitive load, constant voltage or battery load, constant current load or

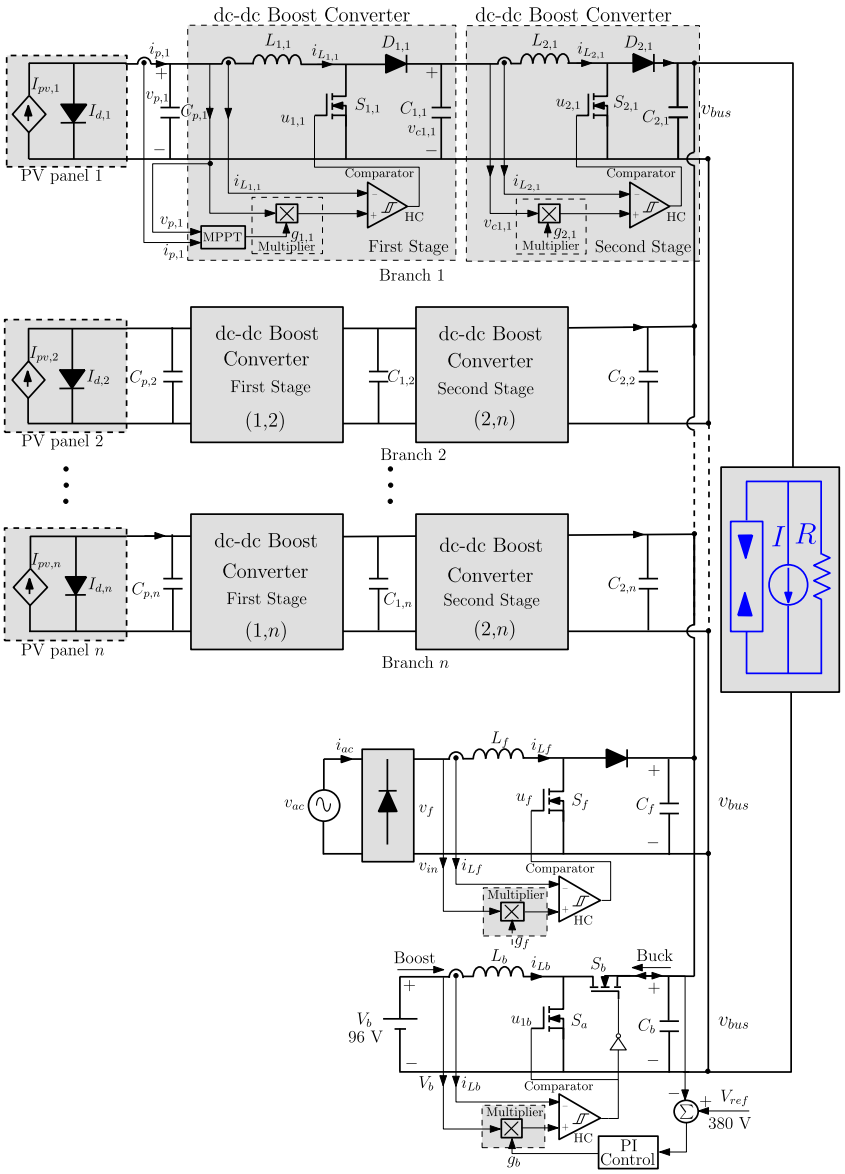

FIGURE 4. Schematic diagram for an example of dc nanogrid supplied a parallel combination of loads (CPL, resistance and constant current load).

linear inductive impedance load. Nevertheless, it has been shown in the literature that in microgrids [37] the load could also be a constant power nature. Therefore, in this paper, the system is supposed to supply a Resistive Load (RL), a Constant Current Load (CCL) and a Constant Power Load (CPL). IN all the cases, for synthesizing the different LFRs, sliding mode control is used.

A possible practical realization of the dc-NG depicted in Fig. 3 is shown in Fig. 4 where the main components have been detailed using their corresponding schematic circuit diagrams.

B. MATHEMATICAL MODELING OF THE DC-NG

In this study, the PV generator model in a branch m is a current source in parallel with a diode (Fig. 4). It can be described by the following equation

$$i_{p,m} = I_{pv,m} - I_{0,m}\left(\exp\left(\frac{v_{p,m}}{AV_{t,m}}\right) - 1\right) \tag{1}$$

where m is an integer number varying from 1 to n labeling the different branches. where $v_{p,m}$ is the voltage of each module, $I_{pv,m}$ and $I_{0,m}$ are the photogenerated and saturation currents for each module, respectively, V_t is the thermal voltage for each PV module which is given by $V_t = N_s KT/q$ where A is the diode ideality factor, K is the Boltzmann constant, q is the charge of the electron, T is the PV module temperature, and N_s is the number of the cells connected in series.

Based on KVL and KCL, the following set of differential equations describing the system of Fig. 4 are obtained

$$\frac{di_{L_{1,m}}}{dt} = \frac{v_{p,m}}{L_{1,m}} - \frac{v_{c1,m}}{L_{1,m}}(1-u_{1,m}) \tag{2a}$$

$$\frac{di_{L_{2,m}}}{dt} = \frac{v_{c1,m}}{L_{2,m}} - \frac{v_{bus}}{L_{2,m}}(1-u_{2,m}) \tag{2b}$$

$$\frac{dv_{p,m}}{dt} = \frac{i_{p,m}}{C_{p,m}} - \frac{i_{L_{1,m}}}{C_{p,m}} \tag{2c}$$

$$\frac{dv_{c1,m}}{dt} = \frac{i_{L_{1,m}}}{C_{1,m}}(1-u_{1,m}) - \frac{i_{L_{2,m}}}{C_{1,m}} \tag{2d}$$

$$\frac{dv_{bus}}{dt} = \sum_{m=1}^{m=n} \frac{i_{L_{2,m}}}{C}(1-u_{2,m}) + \frac{i_{L_b}}{C}(1-u_b) + \frac{i_{L_f}}{C}(1-u_f) - \frac{P}{v_{bus}C} - \frac{I}{C} - \frac{v_{bus}}{RC} \tag{2e}$$

All the parameters that appear in (2a)-(2e) are shown in Fig. 4. Variables $u_{1,m}$, $u_{2,m}$, u_f and u_b are the discontinuous control signals for the different converters and are shown in the same figure. R is the resistance of the load RL, I is the current of load CCL and P is the power of load CPL. The capacitor C is the parallel equivalent capacitance of the different output capacitances in each branch. For simplicity, it is assumed that all the capacitances in the different branches have negligible ESR and the dc bus has a negligible impedance in such a way that $v_{c2,1} = v_{c2,2} = ... = v_{c2,n} = v_{cb} = v_{bus}$. Therefore, the equivalent capacitance at the dc bus terminal can be expressed by $C = C_b + C_f + C_{2,1} + C_{2,2} + ...C_{2,n}$.

Note that the equation describing the dynamical behavior of the dc bus voltage v_{bus} of the dc NG depends on the inductor current i_{L_b} of the BDC and the inductor current i_{L_f} of the PFC converter.

Each branch of two cascaded boost converters is controlled using their corresponding SMC by appropriately selecting their sliding surfaces. The sliding surface in the first stage is described by a switching function $s_{1,m}(\mathbf{x})$, which constraints the relationship between the input voltage of the module $v_{p,m}$ and the input current $i_{L_{1,m}}$. In turn, the sliding surface for the second stage is described by a switching function $s_{2,m}(\mathbf{x})$ which imposes a proportionality between the intermediate voltage $v_{c1,m}$ and the intermediate current $i_{L_{2,m}}$. Therefore, the previous switching functions can be selected as follows

$$s_{1,m}(\mathbf{x}) = g_{1,m}v_{p,m} - i_{L_{1,m}} \tag{3a}$$

$$s_{2,m}(\mathbf{x}) = g_{2,m}v_{c1,m} - i_{L_{2,m}} \tag{3b}$$

where $g_{1,m}$ is the output of the MPPT controller, which is a slowly varying state variable that is considered constant for simplicity, and $g_{2,m}$ is a constant coefficient whose value can be selected according to design specifications such as regulation of the intermediate bus and efficiency optimization [34]. Their time derivatives can be therefore expressed as follows

$$\dot{s}_{1,m}(\mathbf{x}) = g_{1,m}\frac{dv_{p,m}}{dt} - \frac{di_{L_{1,m}}}{dt} \tag{4a}$$

$$\dot{s}_{2,m}(\mathbf{x}) = g_{2,m}\frac{dv_{c1,m}}{dt} - \frac{di_{L_{2,m}}}{dt} \tag{4b}$$

Note that the control variables $u_{1,m}$ $u_{2,m}$ appear in the expressions of the $\dot{s}_{1,m}$ and $\dot{s}_{2,m}$ through the derivative of the inductor currents $i_{L_{1,m}}$ and $i_{L_{2,m}}$ hence guaranteeing the sliding-mode operation of each stage in the different branches.

C. MODELING THE AC-DC PFC CONVERTER

The ac-dc converter performs the PFC by emulating a resistive behavior at the input port, this being the most known application of LFR. As a result, the rectifier exhibits a unity power factor, which is required to meet relevant harmonic standards (e.g. IEC61000-3-2 [38], [39]). The inductor current i_{Lf} in the input port of the PFC converter is described by the following differential equation

$$\frac{di_{L_f}}{dt} = \frac{v_f}{L_f} - \frac{v_{bus}}{L_f}(1-u_f) \tag{5}$$

To induce the LFR behavior in the ac-dc PFC circuit, the following switching function is selected

$$s_f(\mathbf{x}) = g_f v_f - i_f \tag{6}$$

where g_f is an appropriate conductance that can be adjusted according to the required power from the ac utility. The time derivative of the previous switching function is given by the following expression

$$\dot{s}_f(\mathbf{x}) = g_f\frac{dv_f}{dt} - \frac{di_{Lf}}{dt} \tag{7}$$

where it can be observed that the control variable u_f appears through the derivative of i_{L_f} hence sliding-mode regime is guaranteed also in the ac-dc stage [33].

D. MODELLING THE BIDIRECTIONAL CONVERTER

In our case, the purpose of using a BDC is to connect a storage back-up battery to the dc distribution bus. The converter must have a power flow capability to supply the loads during power shortage. The BDC can also control the power flow direction to charge or discharge the storage battery. Moreover, in this work, one of the main functions of the BDC is to regulate the dc bus voltage. This converter is also controlled to induce LFR behavior using a sliding-mode approach. The conductance g_b of the BDC is generated using a PI controller regulating the bus voltage.

Fig. 5 shows the BDC connected to the rest of the NG where the models of the different elements have been simplified and represented by different kind of loads. Namely, the ac-dc converter and the output of the cascaded boost LFRs in each branch have been represented by constant power sources, P_f provided by the utility and P_{pv} delivered by the PV generators. Other loads in the form of constant current source, constant power load and constant resistance load are also taken into account in the block diagram of Fig. 5.

The BDC works in the buck-mode (charging battery), when the total generated power by the PV panels and the ac utility is higher than the absorbed power by the load p_L. The generated

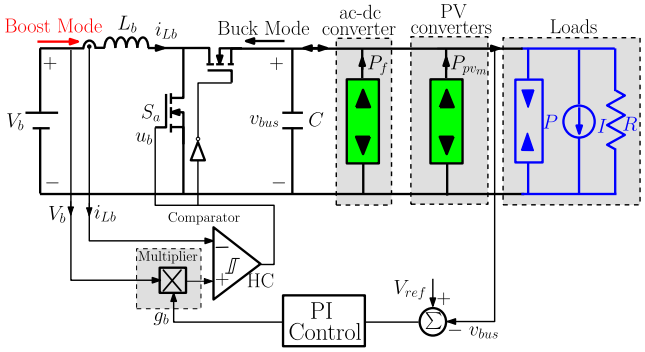

FIGURE 5. Bidirectional converter under sliding-mode control inducing LFR behavior considering the simplified models of the rest of the NG.

power by the PV panels p_{pv}, ac utility p_f and the demanded power by the load p_L can be expressed as follows

$$p_{pv} = p_{o,1} + p_{o,2} + p_{o,3} \ldots + p_{o,n} = \sum_{m=1}^{m=n} p_{o_m} \tag{8}$$

$$p_f = v_f i_{Lf} \tag{9}$$

$$p_L = P + v_{bus} I + \frac{v_{bus}^2}{R} \tag{10}$$

where p_{om} $(m = 1 \ldots n)$ is the power at the output of each branch, P is the power of the constant power load, I is the current of the constant current source and R is the resistance of the resistive load. Similarly, the BDC works in the boost-mode in case of power shortage. The BDC can be modeled as a power source p_s in case of discharging mode or as a power sink p_b in case of charging mode depending on the operating point as it has been explained before. The transferred power of the BDC in both modes can be expressed by the following expressions

$$p_s = p_L - p_{pv} - p_f \quad \text{Discharging mode} \tag{11}$$

$$p_b = p_{pv} + p_f - p_L \quad \text{Charging mode} \tag{12}$$

According to Fig. 5, the BDC working as a boost converter can be expressed using the following set of differential equations

$$\frac{di_{L_b}}{dt} = \frac{V_b}{L_b} - \frac{v_{bus}}{L_b}(1 - u_b) \tag{13}$$

$$\frac{dg_b}{dt} = \frac{\kappa_p}{\tau}(V_{ref} - v_{bus}) - \frac{\kappa_p}{C}\Big(\sum_{m=1}^{m=n} i_{L_{2,m}}(1 - u_{2,m}) + i_{L_f(1-u_f)} + i_{L_b}(1 - u_b) - \frac{P}{v_{bus}} - I - \frac{v_{bus}}{R}\Big) \tag{14}$$

where κ_p is the proportional gain and τ is the time constant of the PI controller.

The BDC is operated as a bidirectional LFR using a sliding-mode approach. Its sliding surface is therefore selected such that a proportionality between the current $i_{L,b}$ and voltage V_b at its input port is imposed. The sliding mode dynamics can be expressed by the switching function $s_b(\mathbf{x})$ as follows

$$s_b(\mathbf{x}) = g_b V_b - i_{L,b} \tag{15}$$

Its time derivative can be expressed as follows

$$\dot{s}_b(\mathbf{x}) = V_b \frac{dg_b}{dt} - \frac{di_{L_b}}{dt} \tag{16}$$

where it can be observed that the control variable u_b appears through the derivative of the inductor current $i_{L,b}$. By controlling the sign of the conductance g_b, the direction of the power flow of the BDC can be fixed. If g_b is positive, the converter works in the discharging boost-mode delivering the power p_s for the dc distribution bus. If g_b is negative, it works in the buck mode to charge the storage battery with power p_b. The power p_s and p_b can be expressed also a function of the conductance g_b as follows

$$p_s = g_b V_b^2 \quad \text{(Boost mode)} \tag{17a}$$

$$p_b = -g_b V_b^2 \quad \text{(Buck mode)} \tag{17b}$$

The conductance parameter g_b is adjusted to regulate the dc bus voltage and can be selected to be the output of the PI dc bus controller as shown in Fig. 5.

III. STABILITY ANALYSIS OF THE DC NANOGRID

To perform a stability analysis of the whole dc-NG, a closed-loop dynamical model is required. This model can be derived by obtaining the expressions of the equivalent control of each element and substituting them in their respective switched models (Eqs. (2a)-(2e), (5) and (13)-(14)) while taking into account the sliding-mode condition (Eqs. (3a)-(4b), (6)-(7) and (15)-(16)). The expression of the equivalent control for each element of the dc-NG can be obtained by equating to zero the corresponding switching functions and solving for the binary signals $u_{1,m}$, $u_{2,m}$, u_f and u_b. Hence, the following expressions for the equivalent control variables $u_{eq_{1,m}}$, $u_{eq_{2,m}}$ and $u_{b_{eq,b}}$ can be obtained

$$u_{eq_{1,m}} = 1 - \frac{v_{d,m}}{v_{c1,m}} \tag{18a}$$

$$u_{eq_{2,m}} = 1 - \frac{v_{c1,m}}{v_{bus}}\left(1 - \alpha_{2,m} g_{2,m}\right) + \frac{g_{1,m} v_{p,m} \alpha_2}{v_{c1,m} v_{bus}} v_{d,m}$$

$$u_{eq,f} = 1 - \frac{v_f}{v_{bus}}\left(1 - \frac{g_f L_f \omega}{\tan(\omega t)}\right) \tag{18b}$$

$$u_{eq,b} = 1 - \frac{L_b C}{V_b i_{Lb} \kappa_p L_b - C v_{bus}}\Big[V_b\Big[\frac{\kappa_p}{\tau}(V_{ref} - v_{bus}) - \frac{\kappa_p}{C}\Big(\sum_{m=1}^{m=n} i_{L_{2,m}}(1 - u_{eq_{2,m}}) + \frac{g_f v_f^2}{v_{bus}} m_f - \frac{P}{v_{bus}} - I - \frac{v_{bus}}{R}\Big)\Big] - \frac{V_b}{L_b}\Big] \tag{18c}$$

where $v_{d,m} = v_{p,m} - \alpha_{1,m}(i_{p,m} - g_{1,m} v_{p,m})$, $\alpha_{1,m} = g_1 L_1 / C_p$, $\alpha_{2,m} = g_{2,m} L_{2,m} / C_{1,m}$ and $m_f = 1 - \dfrac{g_f L_f \omega}{\tan(\omega t)}$.

Introducing (18a)-(18c) into Eqs. (2a)-(2e), (5) and (13)-(14) and considering Eqs. (3a)-(4b) and (15)-(16)

result in the following reduced-order model for the ideal sliding-mode dynamics:

$$\frac{dv_{p,m}}{dt} = \frac{i_{p,m}}{C_{p,m}} - \frac{g_{1,m}v_{p,m}}{C_{p,m}} \tag{19a}$$

$$\frac{dv_{c1,m}}{dt} = \frac{g_{1,m}v_{p,m}^2}{C_{1,m}v_{c1,m}} + \frac{\alpha_{1,m}g_{1,m}v_{p,m}}{C_{1,m}v_{c1,m}}(g_{1,m}v_{p,m} - i_{p,m}) - \frac{g_{2,m}v_{c1,m}}{C_{1,m}} \tag{19b}$$

$$\frac{dv_{bus}}{dt} = \sum_{m=1}^{m=n} \frac{i_{L_{2,m}}}{C}\left(\frac{v_{c1,m}}{v_{bus}}(1-\alpha_{2,m}g_{2,m}) + \frac{g_{1,m}v_{p,m}}{v_{c1,m}}v_{d,m}\right) + \frac{g_f v_f^2}{v_{bus}}(1 - \frac{g_f L_f \omega}{\tan(\omega t)}) + \frac{i_{L_b}}{C}\frac{V_b}{v_{bus}} - \frac{P}{v_{bus}C} - \frac{I}{C} - \frac{v_{bus}}{RC} \tag{19c}$$

$$\frac{dg_b}{dt} = \frac{\kappa_p}{\tau}(V_{ref} - v_{bus}) - \frac{\kappa_p}{C}\left(\sum_{m=1}^{m=n} i_{L_{2,m}}(1-u_{eq_{2,m}}) + \frac{g_f v_f^2}{v_{bus}}(1 - \frac{g_f L_f \omega}{\tan(\omega t)}) + i_{L_b}(1-u_{b_{eq,b}}) - \frac{P}{v_{bus}} - I - \frac{v_{bus}}{R}\right) \tag{19d}$$

Note that the state equations describing the dc distribution voltage and the conductance depend on the ac utility line frequency which is well below the switching frequency. Therefore, the rectified ac input voltage at the PFC converter can be considered constant during few consecutive switching periods [40]. The term $g_f v_f^2(1 - g_f L_f \omega/\tan(\omega t))$ can be approximated to its dc averaged value $g_f V_f^2$ over one line period, where V_f is the dc component of the rectified sinusoidal voltage v_f.

Using the reduced order model (19a)-(19d) and taking into account the constraints imposed by the sliding surfaces, the equilibrium point of the system is expressed as follows

$$x^* = [V_{p,m}, V_{c1,m}, v_{bus}, G_b]^\intercal = [\frac{I_{e,m}}{G_{1,m}}, \frac{I_{e,m}}{\sqrt{G_{1,m}G_{2,m}}}, V_{ref}, \frac{P_s}{V_b^2}]^\intercal \tag{20}$$

where

$$I_{e,m} = I_{pv,m} + I_{0,m} - G_{1,m}V_{t,m}\mathcal{W}\left(\frac{I_{0,m}\exp\left(\frac{I_{pv,m}+I_{0,m}}{G_{1,m}V_{t,m}}\right)}{G_{1,m}V_{t,m}}\right) \tag{21}$$

where $\mathcal{W}$ stands for the Lambert-W function and P_s is the supplied power from the storage battery to the downstream loads at the equilibrium point $P_s = -P_b = P_L - P_{pv} - P_f$. The load power, generated PV power and ac utility power at the equilibrium point can be redefined as follows

$$P_L = P + IV_{ref} + \frac{V_{ref}^2}{R} \tag{22a}$$

$$P_{pv} = \sum_{m=1}^{m=n} \frac{I_{e,m}^2}{G_{1,m}} \tag{22b}$$

$$P_f = g_f V_f^2 \tag{22c}$$

Let $\mathbf{J}$ be the Jacobian matrix of (19a)-(19d) and $\mathbf{I}$ be a unitary matrix with appropriate size. Therefore, the characteristic polynomial equation $\det(\mathbf{J} - s\mathbf{I})$ can be expanded in the following form

$$\prod_{m=1}^{m=n}(s + \frac{G_{1,m}}{C_{p,m}})(s + \frac{2G_{2,m}}{C_{1,m}})(s^2 + a_1 s + a_0) = 0 \tag{23}$$

where a_1 and a_0 can be defined as follows

$$a_1 = \frac{\tau(\kappa_p V_b^2 + I + 2V_{ref}/R) - \kappa_p L_b P_s}{\tau(CV_{ref} - \kappa_p L_b P_s)} \tag{24a}$$

$$a_0 = \frac{\kappa_p V_b^2}{\tau(CV_{ref} - \kappa_p L_b P_s)} \tag{24b}$$

Note that the characteristic polynomial has $2n + 2$ roots. Namely, $2n$ roots correspond to the n branches of the PV-fed two-stage boost converters and two roots for the BDC. It can be observed that the roots corresponding to the n branches are located in the left half side of the complex plane. Those corresponding to the BDC can be appropriately selected to ensure the desired system performances. For the system to be stable, the following conditions must be fulfilled

$$\kappa_p < \frac{CV_{ref}}{L_b P_s} \quad \text{and } \tau > \frac{L_b P_s}{V_b^2} \tag{25}$$

As mentioned before, the BDC is responsible for the regulation of the dc bus and the power flow direction in the BDC. Therefore, the PI controller for this converter should be appropriately designed. With this aim, a small-signal model is needed, which can be derived by first obtaining the large-signal model from the switched model of the converter, assuming the sliding mode condition and using the expression of the equivalent control. The switched model was given in (13)-(14) and Eq. (2e). From (2e), the equivalent control of the BDC can be expressed as follows:

$$u_{b,eq} = 1 - \frac{C}{i_{L_b}}\frac{dv_{bus}}{dt} + \sum_{m=1}^{m=n}\frac{i_{L_{2,m}}}{i_{L_b}}(1-u_{eq2,m}) + i_{L_f}(1-u_{eq,f}) - \frac{P}{i_{L_b}v_{bus}} - \frac{i}{i_{L_b}} - \frac{v_{bus}}{Ri_{L_b}} \tag{26}$$

From the switching conditions of Eq. (15), (16), the inductor current of the BDC can be expressed as follows

$$i_{L_b} = g_b V_b \tag{27}$$

By substituting Eqs. (26), (27) (13), the following equation is obtained

$$g_b v_b^2 \frac{dg_b}{dt} = \frac{g_b v_b^2}{L_b} - \frac{v_{bus}}{L_b}(C\frac{dv_{bus}}{dt} - \sum_{m=1}^{m=n} i_{L_{2,m}}(1-u_{eq2,m}) - i_{L_f}(1-u_{eq,f}) + \frac{P}{v_{bus}} + i + \frac{v_{bus}}{R}) \tag{28}$$

The previous equation describes the large-signal low-frequency characteristics of the BDC operating as a LFR.

The small-signal transfer functions of the BDC can be derived by linearizing the large-signal model and taking the Laplace transform of the resulting equations [41]. In the following analysis, it will be assumed that the uppercase letter denotes the steady-state value of a variable, the lowercase letter denotes the averaged value of the same variable, and the lowercase letter with a hat denotes the small-signal disturbance close to the steady-state value. Therefore, it can be written as follows

$$v_b = V_b + \hat{v}_b, \quad g_b = G_b + \hat{g}_b \tag{29a}$$
$$v_{p,m} = V_{p,m} + \hat{v}_{p,m}, \quad v_{c1,m} = V_{c1,m} + \hat{v}_{c1,m} \tag{29b}$$
$$v_{bus} = v_{bus} + \hat{v}_{bus}, \quad i = I + \hat{i} \tag{29c}$$
$$v_f = V_f + \hat{v}_f. \tag{29d}$$

By substituting the previous expressions in Eq. (28), keeping only first-order terms and taking into account that the time-derivatives of the steady-state value are zero, the Laplace domain model can be obtained. The resulting expression of the disturbed dc bus voltage can be expressed as follows

$$\hat{v}_{bus} = G_{v,g_b}\hat{g}_b + G_{v,v_b}\hat{v}_b + G_{v,i}\hat{i} + G_{v,v_f}(s)\hat{v}_f + \sum_{m=1}^{m=n}(G_{v,v_{pm}}\hat{v}_{p,m} + G_{v,v_{cm}}\hat{v}_{c1,m}), \tag{30}$$

where G_{v,g_b}, G_{v,v_b}, $G_{v,i}$, G_{v,p_m} and G_{v,c_m} can be expressed as follows

$$G_{v,g_b}(s) = \frac{\hat{v}_{bus}(s)}{\hat{g}_b(s)} = \frac{b_1 s + b_2}{s + a} \tag{31a}$$
$$G_{v,v_b}(s) = \frac{\hat{v}_{bus}(s)}{\hat{v}_b(s)} = \frac{b_3}{s + a} \tag{31b}$$
$$G_{v,i}(s) = \frac{\hat{v}_{bus}(s)}{\hat{i}(s)} = \frac{-1/C}{s + a} \tag{31c}$$
$$G_{v,v_{pm}}(s) = \frac{\hat{v}_{bus}(s)}{\hat{v}_{p,m}(s)} = \frac{2\alpha_2 G_{1,m} V_{p,m}}{V_{c1,m}(s + a)} \tag{31d}$$
$$G_{v,v_{c1m}}(s) = \frac{\hat{v}_{bus}(s)}{\hat{v}_{c_1,m}(s)} = \frac{1 - G_{2,m}\alpha_{2,m} - \frac{\alpha_{2,m} G_{1,m} V_{p,m}^2}{V_{c1,m}^2}}{(s + a)} \tag{31e}$$
$$G_{v,v_f}(s) = \frac{\hat{v}_{bus}(s)}{\hat{v}_f(s)} = \frac{2 g_f V_f}{C V_{ref}(s + a)} \tag{31f}$$

where in turn, the parameters a, b_1, b_2 and b_3 are defined as follows $a = 2/(RC) + I/(CV_{ref})$, $b_1 = -L_b P_s/(CV_{ref})$, $b_2 = V_b^2/(CV_{ref})$ and $b_3 = 2(P_L - P_{pv})/(CV_b V_{ref})$.

In order to regulate the voltage of the dc distribution bus, the transfer function $G_{v,g_b}(s)$ should be considered since it represents the relationship between the dc bus voltage $\hat{v}_{bus}(s)$ and the control variable $\hat{g}_b(s)$. The closed-loop dynamic model for the BDC is shown in Fig. 6 with all the elements of the dc-NG. The transfer function $G_c(s)$ of the PI compensator

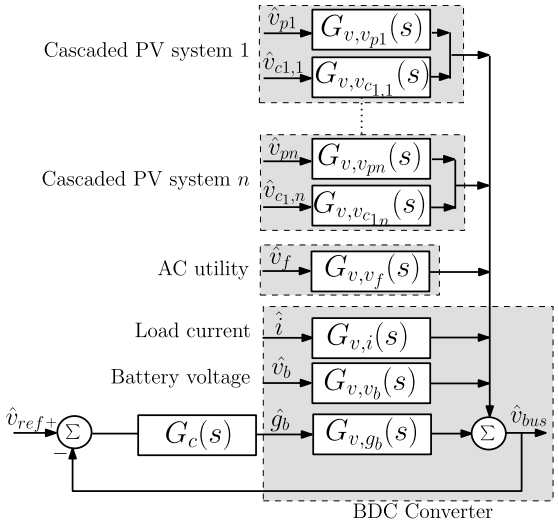

FIGURE 6. Small signal block diagram for the BDC based on SLFR considering the rest of the dc-NG.

can be expressed in the following form:

$$G_c(s) = \frac{\kappa_p(\tau s + 1)}{s\tau} \tag{32}$$

To simplify the design of the controller, the pole in Eq. (31a) of the BDC is canceled by the zero of the PI compensator of Eq. (32). The gain κ_p and the time constant τ of the PI controller has been selected such that the system presents a phase margin of 45^o. Using Eq. (31a) and Eq. (32), and taking into account the pole-zero cancellation, the total loop transfer function $\mathcal{T}(s)$ of the system can be expressed as follows

$$G_c(s) = \frac{\kappa_p(b_1 s + b_2)}{s} \tag{33}$$

This model can be used to design the system with the desired closed-loop performances.

Referring to Fig. 6, the closed loop $\hat{i}$-to-$\hat{v}_{bus}$ transfer function can be written as follows

$$G_{v,ic}(s) = -\frac{\frac{1}{C}}{s + a}\frac{\mathcal{T}(s)}{1 + \mathcal{T}(s)} \tag{34}$$

which can be expressed in the following canonical form

$$G_{v,i_c}(s) = \frac{-W_1(s + \frac{b_2}{b_1})}{s^2 + 2\zeta\omega_n s + \omega_n^2} \tag{35}$$

where W_1, W_2, ω_n and ζ are as follows:

$$W_1 = \frac{\kappa_p b_1}{C(1 + \kappa_p b_1)}, \quad W_2 = \frac{2 g_f V_f b_1 \kappa_p}{C V_{ref}(1 + \kappa_p b_1)} \tag{36a}$$
$$\omega_n = \sqrt{\frac{a\kappa_p b_2}{1 + \kappa_p b_1}} \tag{36b}$$
$$\zeta = \frac{\kappa_p b_2 + a(1 + \kappa_p b_1)}{2\omega_n(1 + \kappa_p b_1)} \tag{36c}$$

TABLE 1. The used parameter values for the proposed dc-NG.

$L_{1,m}$	$L_{2,m}$	L_b	$C_{p,m}$	$C_{1,m}$	C	$g_{2,m}$	κ_p	τ
200 μH	2 mH	0.62 mH	100 μF	10 μF	430 μF	0.008 S	0.0005	0.03 s

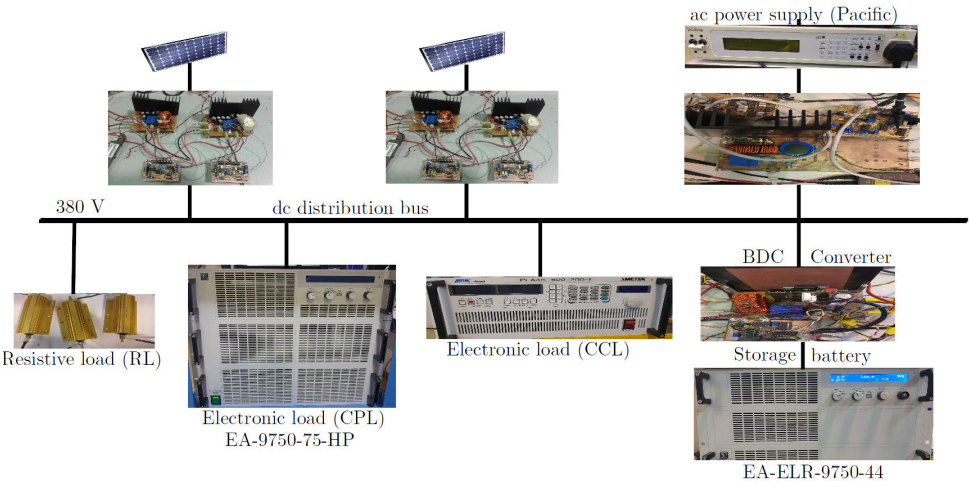

FIGURE 7. Experimental setup for the implemented dc-NG.

Similarly, the closed loop $\hat{v}_f$-to-$\hat{v}_{bus}$ transfer function can expressed as follows

$$G_{v,v_{fc}}(s) = \frac{W_2(s + \frac{b_2}{b_1})}{s^2 + 2\zeta\omega_n s + \omega_n^2} \tag{37}$$

Using the previous parameters, the settling time $t_s = 4/(\zeta\omega_n)$ and the maximum overshoot $M_a = \exp^{-\pi\zeta/\sqrt{1-\zeta^2}}$ can be calculated.

IV. NUMERICAL SIMULATIONS AND EXPERIMENTAL RESULTS

In this section, a validation of the previous theoretical results using numerical simulations and experimental results are presented. A system consisting of two PV panels, an ac source and a storage battery are connected to synthesize a dc-NG as shown in Fig. 7. These power sources are connected to the dc bus of the dc-NG through different converters operating as LFRs. A battery of 96 V has been used as an energy storage and has been connected to the dc bus using a BDC. The PV panels have been used to feed the dc bus through two cascaded boost converters operating as LFRs and the ac source has fed the dc bus using an ac-dc converter. The considered PV generator here has a nominal power of 85 W and its parameters are listed in [42]. The dc-NG has been loaded by a parallel combination of different loads, Constant Power Load (CPL), Constant Current Load (CCL) and a Constant Resistance Load (CRL). Two electronic loads have been used in the experimental set-up, the first one working as a CPL and the second one as CCL. The used equipments are illustrated in Fig. 7. Table 1 shows the parameter values used in the numerical simulations and experimental setup.

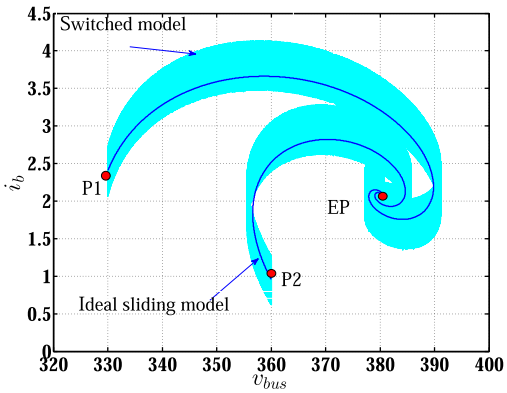

FIGURE 8. Trajectories of two cascaded boost-based LFRs starting from different initial conditions in the plane (i_{Lb}; v_{dc}) for κ_p= 0.0005, τ= 0.03 s.

Firstly, the validity of the ideal sliding dynamic model is verified by numerical simulation by comparing the results from this model and those from the full-order detailed switched model implemented in PSIM © software in different regions of the state space. As depicted in Fig. 8, two initial conditions P1 and P2 are considered while the system is simulated using the two different models. It can be observed from this figure that there is a good matching between the two models both in transient and in steady-state operation.

Secondly, the system has been checked under a step change of input power using numerical simulations and experimental results and the results are depicted in Fig. 9.

The supplied power by the ac source reduces from 600 W (Interval A) to 200 W (Interval B) for a total load power of 500 W. The supplied power by the PV panels is equal to 100 W. The total load power has been distributed among

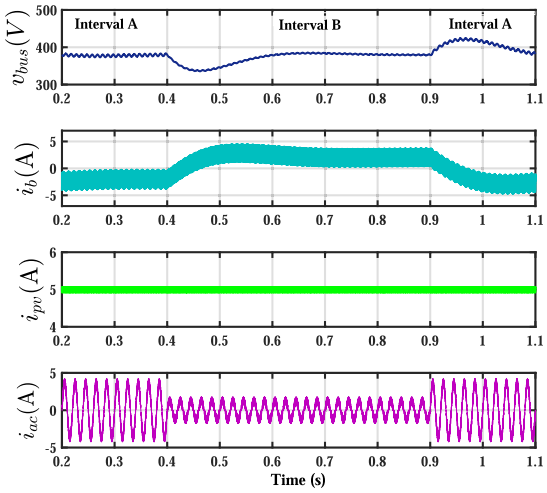

(a) Numerical simulation

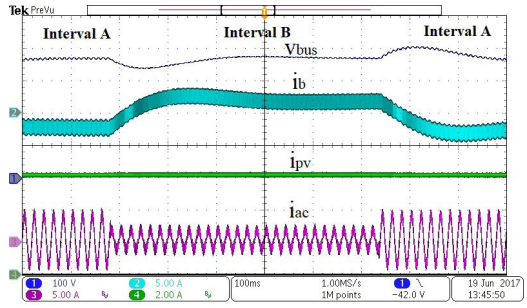

(b) Experimental results.

FIGURE 9. Corresponding waveforms of the dc-NG when the input power for the PV panels equals 100 W and the power of the ac utility changes from 600 W (Interval A) to 200 W (Interval B) under load of 500 W.

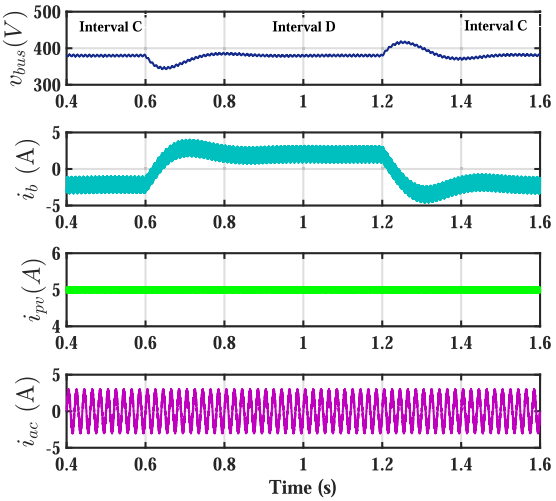

(a) Numerical simulation

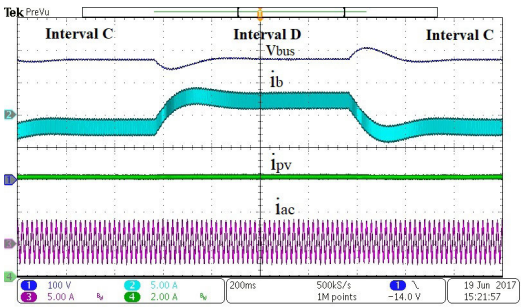

(b) Experimental results

FIGURE 10. Corresponding waveforms of the dc-NG under CCL change from 100 W (Interval C) to 500 W (Interval D), 100 W for the CPL and 100 W for the RL under fixed input power of 500 W.

different kinds of loads, an RL of 1423 Ω which is equivalent to 100 W, a CCL of 0.53 A which is equivalent to 200 W and a CPL of 200 W. Note that during the interval A, the supplied power is enough for the load because the total input power is equal to 700 W which includes the PV power and PFC power. The BDC in that moment operates in buck mode to charge the storage battery. On the other hand, for interval B, when the input power decreases from 600 W to 200 W, the generated power is not enough to feed the required power by the load because the total input power is equal to 300 W. Thus, the BDC operates in boost mode to compensate the lack of power which must be provided by the battery. Note also that under input power disturbances, the dc bus exhibits a recovery to its steady-state value with a settling time around 330 ms and an overshoot voltage 40 V that means around 10%

The system has been also checked under a step load change and fixed input power. The total load power has been distributed among different kinds of loads, an RL of 1423 Ω which is equivalent to 100 W, a CCL of 0.26 A which is equivalent to 100 W and a CPL of 100 W. The generated power by the PFC and PV panels have been fixed to 400 W and 100 W respectively. Therefore, the total input power to the dc-NG is equal to 500 W. The load power changes from 300 W (Interval C) to 700 W (Interval D) by changing the CCL power from 100 W to 500 W. In this test the load power was distributed among three different kinds of loads. Namely, an RL and a CPL whose power has been both maintained fixed to 100 W in both a CCL whose power has been changed from 100 W (Interval C) to 500 W (Interval D). Fig. 10 shows the corresponding simulated and experimental waveforms. Note that when the required power by the load is equal to 300 W, the input power is enough to supply the load and the extra generated power is used to charge the battery through the BDC which operates in the buck-mode. However, when the load power changes from 300 W to 700 W, the total generated input power (500 W) is not enough to supply the load and in this case, the sign of the conductance g_b of the BDC is inverted automatically by the controller. Then, the power flow in the BDC is changed causing this converter to operate in the boost mode. Note that under load power changes, the dc bus exhibits a fast recovery with similar settling time and overshoot as in the previous case.

A state space trajectory of the BDC under load change with a total input power of 500 W is depicted in Fig. 11, which was obtained from numerical simulations using the detailed switched model and from experimental measurements in the

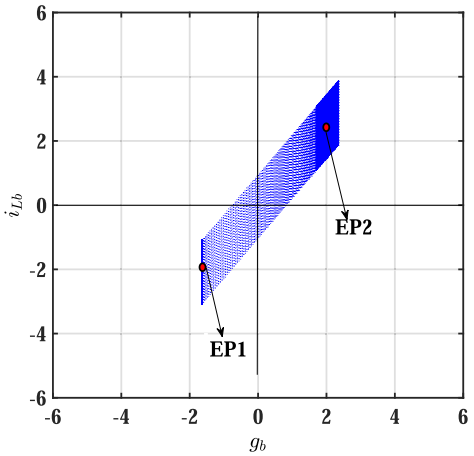

(a) Numerical simulation

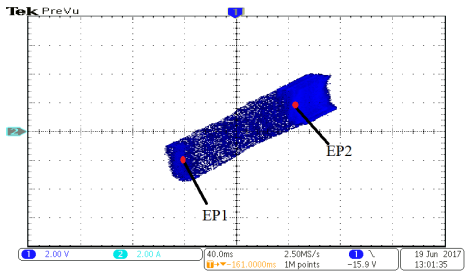

(b) Experimental results

FIGURE 11. Trajectories in the state plane (i_{Lb}, g_b) of the BDC under load change.

TABLE 2. Design criteria for the dc-NG in terms of damping ratio ζ, natural angular frequency ω_n, settling time t_s and maximum overshoot M_a.

ζ	ω_n	t_s	M_a
0.5773	21.05 rad/s	329.1 ms	10.85%

laboratory prototype. This figure shows both transient and steady-state operation of the BDC when it works in different modes. When the load power is equal to 300 W, the BDC operates in the buck mode and its average steady-state correspond to Point EP1. When the load power is equal to 700 W, the BDC operates in the boost mode and its average steady-state moves to Point EP2.

Using the previous parameters, the settling time $t_s = 4/(\zeta\omega_n)$ and the maximum overshoot $M_a = \exp^{-\pi\zeta/\sqrt{1-\zeta^2}}$ have been calculated and the results are listed in Table. 2. As can be observed, the theoretical results are in a remarkable agreement with the numerical simulations and the experimental measurements.

V. CONCLUSION

In this paper, a modular PV household dc nanogrid has been proposed. The novelty lies in the synthesis and implementation of the nanogrid using converters with LFR behavior in all the elements of the network. The latter consists of three canonical elements, namely, a rectifier block supplied by the AC grid, a bidirectional converter with a battery, and several unidirectional converters each of them supplied by a PV generator. The main features of resulting network are the following:

i) The LFR behavior in the converters processing the solar energy allows the straightforward paralleling of their outputs ports.

ii) The LFR nature of the rectifier provides power factor correction

iii) The LFR characteristics in the bidirectional converter establish the operating modes, i.e., battery discharge when the LFR emulated resistor is positive and battery charge when it is negative.

iv) The stability of the interconnected blocks is ensured by a simple feedback loop in the bidirectional converter, which regulates the DC bus voltage.

REFERENCES

[1] B. Fahimi, A. Kwasinski, A. Davoudi, R. S. Balog, and M. Kiani, "Powering a more electrified planet," *IEEE Power Energy Mag.*, no. 2, pp. 54–64, Mar. 2011.

[2] B. N. Alajmi, K. H. Ahmed, S. J. Finney, and B. W. Williams, "A maximum power point tracking technique for partially shaded photovoltaic systems in microgrids," *IEEE Trans. Ind. Electron.*, vol. 60, no. 4, pp. 1596–1606, Apr. 2013.

[3] P. Muthuvel, S. A. Daniel, and D. G. Yazhini, "Retrofitting domestic appliances for PV powered DC Nano-grid and its impact on net zero energy homes in rural India," *Eng. Sci. Technol., Int. J.*, vol. 19, no. 4, pp. 1836–1844, Dec. 2016.

[4] P. Muthuvel, S. Arul Daniel, and S. K. Paul, "Sizing of PV array in a DC nano-grid for isolated households after alteration in time of consumption," *Eng. Sci. Technol., Int. J.*, vol. 20, no. 6, pp. 1632–1641, Dec. 2017.

[5] M. Nasir, H. A. Khan, A. Hussain, L. Mateen, and N. A. Zaffar, "Solar PV-based scalable DC microgrid for rural electrification in developing regions," *IEEE Trans. Sustain. Energy*, vol. 9, no. 1, pp. 390–399, Jan. 2018.

[6] C. Cabal, F. Guinjoan, C. Alonso, L. Martínez-Salamero, and L. Séguier, "Maximum power point tracking based on sliding-mode control for output-series connected converters in photovoltaic systems," *IET Power Electron.*, vol. 7, no. 4, pp. 914–923, Apr. 2014.

[7] E. Planas, A. Gil-de-Muro, J. Andreu, I. Kortabarria, and I. M. de Alegría, "Design and implementation of a droop control in D-Q frame for islanded microgrids," *IET Renew. Power Generat.*, vol. 7, no. 5, pp. 458–474, Sep. 2013.

[8] L. de S. Ribeiro, O. Saavedra, S. de Lima, and J. G. de Matos, "Isolated micro-grids with renewable hybrid generation: The case of Lencois island," *IEEE Trans. Sustain. Energy*, vol. 2, no. 1, pp. 1–11, Jan. 2011.

[9] H. H. Sathler, L. H. Sathler, F. L. F. Marcelino, T. R. de Oliveira, S. I. Seleme, and P. F. D. Garcia, "A comparative efficiency study on bidirectional grid interface converters applied to low power DC nanogrids," in *Proc. Brazilian Power Electron. Conf. (COBEP)*, Nov. 2017, pp. 1–6.

[10] K. Sun, L. Zhang, Y. Xing, and J. M. Guerrero, "A distributed control strategy based on DC bus signaling for modular photovoltaic generation systems with battery energy storage," *IEEE Trans. Power Electron.*, vol. 26, no. 10, pp. 3032–3045, Oct. 2011.

[11] P. Sintupatsuk, S. Khomfoi, and P. Paisuwanna, "A DC to DC multilevel modular capacitor clamped converter with electrical grounding isolation and bidirectional power flow for a DC microgrid application," in *Proc. 9th Int. Conf. Electr. Eng./Electron., Comput., Telecommun. Inf. Technol.*, May 2012, pp. 1–4.

[12] E. Lenz and D. J. Pagano, "Nonlinear control for bidirectional power converter in a DC microgrid," *IFAC Proc. Volumes*, vol. 46, no. 23, pp. 359–364, 2013.

[13] V. Stramosk and D. J. Pagano, "Nonlinear control of a bidirectional DC-DC converter operating with boost-type Constant-Power Loads," in *Proc. Brazilian Power Electron. Conf.*, Oct. 2013, pp. 305–310.

[14] J. A. Barrado, A. E. Aroudi, H. Valderrama-Blavi, J. Calvente, and L. Martinez-Salamero, "Analysis of a self-oscillating bidirectional DC–DC converter in battery energy storage applications," *IEEE Trans. Power Del.*, vol. 27, no. 3, pp. 1292–1300, Jul. 2012.
[15] S. Peyghami, H. Mokhtari, and F. Blaabjerg, "Autonomous operation of a hybrid AC/DC microgrid with multiple interlinking converters," *IEEE Trans. Smart Grid*, vol. 9, no. 6, pp. 6480–6488, Nov. 2018.
[16] X. Lu, J. M. Guerrero, K. Sun, and J. C. Vasquez, "An improved droop control method for DC microgrids based on low bandwidth communication with DC bus voltage restoration and enhanced current sharing accuracy," *IEEE Trans. Power Electron.*, vol. 29, no. 4, pp. 1800–1812, Apr. 2014.
[17] S. Peyghami, H. Mokhtari, and F. Blaabjerg, "Autonomous power management in LVDC microgrids based on a superimposed frequency droop," *IEEE Trans. Power Electron.*, vol. 33, no. 6, pp. 5341–5350, Jun. 2018.
[18] L. Xu and D. Chen, "Control and operation of a DC microgrid with variable generation and energy storage," *IEEE Trans. Power Del.*, vol. 26, no. 4, pp. 2513–2522, Oct. 2011.
[19] P. Shanthi, D. Parvathyshankar, and U. Govindarajan, "Instantaneous power-based current control scheme for VAR compensation in hybrid AC/DC networks for smart grid applications," *IET Power Electron.*, vol. 7, no. 5, pp. 1216–1226, May 2014.
[20] S. Sanchez, A. H. Soloot, and M. Molinas, "Stability influence of renewable energy systems: Connection to DC nanogrids," in *Proc. IEEE 17th Workshop Control Model. Power Electron. (COMPEL)*, Trondheim, Norway, Jun. 2016, pp. 1–8.
[21] X. Yue, D. Boroyevich, F. C. Lee, F. Chen, R. Burgos, and F. Zhuo, "Beat frequency oscillation analysis for power electronic converters in DC nanogrid based on crossed frequency output impedance matrix model," *IEEE Trans. Power Electron.*, vol. 33, no. 4, pp. 3052–3064, Apr. 2018.
[22] R. D. Middlebrook, "Power electronics: An emerging discipline," in *Proc. Adv. Switched-Mode Power Convers.*, 1981, pp. 11–15.
[23] S. Singer, "Loss-free gyrator realization," *IEEE Trans. Circuits Syst.*, vol. 35, no. 1, pp. 26–34, Jan. 1988.
[24] S. Singer, "Realization of loss-free resistive elements," *IEEE Trans. Circuits Syst.*, vol. 37, no. 1, pp. 54–60, Jan. 1990.
[25] S. Singer and R. W. Erickson, "Canonical modeling of power processing circuits based on the POPI concept," *IEEE Trans. Power Electron.*, vol. 7, no. 1, pp. 37–43, Jan. 1992.
[26] S. Luo, "A review of distributed power systems part I: DC distributed power system," *IEEE Aerosp. Electron. Syst. Mag.*, vol. 20, no. 8, pp. 5–16, Aug. 2005.
[27] A. Cid-Pastor, L. Martinez-Salamero, C. Alonso, R. Leyva, and S. Singer, "Paralleling DC–DC switching converters by means of power gyrators," *IEEE Trans. Power Electron.*, vol. 22, no. 6, pp. 2444–2453, Nov. 2007.
[28] R. Haroun, A. Cid-Pastor, A. El Aroudi, and L. Martinez-Salamero, "Synthesis of canonical elements for power processing in DC distribution systems using cascaded converters and sliding-mode control," *IEEE Trans. Power Electron.*, vol. 29, no. 3, pp. 1366–1381, Mar. 2014.
[29] A. Marcos-Pastor, E. Vidal-Idiarte, A. Cid-Pastor, and L. Martinez-Salamero, "Loss-free resistor-based power factor correction using a semi-bridgeless boost rectifier in sliding-mode control," *IEEE Trans. Power Electron.*, vol. 30, no. 10, pp. 5842–5853, Oct. 2015.
[30] A. Marcos-Pastor, E. Vidal-Idiarte, A. Cid-Pastor, and L. Martinez-Salamero, "Interleaved digital power factor correction based on the sliding-mode approach," *IEEE Trans. Power Electron.*, vol. 31, no. 6, pp. 4641–4653, Jun. 2016.
[31] A. Cid-Pastor, L. Martinez-Salamero, C. Alonso, A. El Aroudi, and H. Valderrama-Blavi, "Power distribution based on gyrators," *IEEE Trans. Power Electron.*, vol. 24, no. 12, pp. 2907–2909, Dec. 2009.
[32] A. Cid-Pastor, L. Martinez-Salamero, R. Leyva, J. Calvente, and R. Giral, "Design of photovoltaic-based current sources for maximum power transfer by means of power gyrators," *IET Power Electr.*, vol. 4, no. 6, p. 674, 2011.
[33] A. Cid-Pastor, L. Martinez-Salamero, A. El Aroudi, R. Giral, J. Calvente, and R. Leyva, "Synthesis of loss-free resistors based on sliding-mode control and its applications in power processing," *Control Eng. Pract.*, vol. 21, no. 5, pp. 689–699, May 2013.
[34] R. Haroun, A. El Aroudi, A. Cid-Pastor, G. Garcia, C. Olalla, and L. Martinez-Salamero, "Impedance matching in photovoltaic systems using cascaded boost converters and sliding-mode control," *IEEE Trans. Power Electron.*, vol. 30, no. 6, pp. 3185–3199, Jun. 2015.
[35] Z. Yongqiang and W. Tianjing, "Comparison of centralised and distributed energy storage configuration for AC/DC hybrid microgrid," *J. Eng.*, vol. 2017, no. 13, pp. 1838–1842, Jan. 2017.
[36] Y. Gu, X. Xiang, W. Li, and X. He, "Mode-adaptive decentralized control for renewable DC microgrid with enhanced reliability and flexibility," *IEEE Trans. Power Electron.*, vol. 29, no. 9, pp. 5072–5080, Sep. 2014.
[37] A. Kwasinski and C. N. Onwuchekwa, "Dynamic behavior and stabilization of DC microgrids with instantaneous constant-power loads," *IEEE Trans. Power Electron.*, vol. 26, no. 3, pp. 822–834, Mar. 2011.
[38] *IEEE Recommended Practices and Requirements for Harmonic Control in Electrical Power Systems*, IEEE Standard 519-1992, Apr. 1993.
[39] *Limits for Harmonic Current Emissions (Equipment Input Current ≤ 16 A Per Phase)*, document IEC 61000-3-2, Part 3–2, 3rd ed., 2005.
[40] M. Bodetto, A. El Aroudi, A. Cid-Pastor, J. Calvente, and L. Martinez-Salamero, "Design of AC-DC PFC high-order converters with regulated output current for low-power applications," *IEEE Trans. Power Electron.*, vol. 31, no. 3, pp. 2012–2025, Mar. 2016.
[41] Y.-F. Liu and P. C. Sen, "Large-signal modeling of hysteretic current-programmed converters," *IEEE Trans. Power Electron.*, vol. 11, no. 3, pp. 423–430, May 1996.
[42] *BP Solar BP585 Datasheet*. [Online]. Available: http://www.electricsystems.co.nz/documents/BPSolar85w.pdf

REHAM HAROUN (Member, IEEE) was born in Egypt, in 1982. She received the bachelor's degree in power and electrical engineering and the master's degree from the Aswan Faculty of Engineering, South Valley University, Aswan, Egypt, in 2004 and 2009, respectively, and the Ph.D. degree with Universitat Rovira i Virgili, Tarragona, Spain, in 2014. She was a Lecture Assistant with the South Valley University, from 2004 to 2009. From 2004 to 2009, she was a member of the Aswan Power Electronics Application Research Center (APEARC) Group. She is currently a member of the GAEI Research Group (Universitat Rovira i Virgili) on industrial electronics and automatic control whose main research fields are power electronics applications, including dc-dc switched power supply and ac-dc power factor correction circuits.

ABDELALI EL AROUDI (Senior Member, IEEE) received the bachelor's degree in physical science from the Faculté des Sciences, Université Abdelmalek Essaadi, Tetouan, Morocco, in 1995, and the Ph.D. degree (Hons.) in applied physical science from the Universitat Politècnica de Catalunya, Barcelona, Spain, in 2000. From 1999 to 2001, he was a Visiting Professor with the Department of Electronics, Electrical Engineering and Automatic Control, Technical School, Universitat Rovira i Virgili (URV), Tarragona, Spain, where he became an Associate Professor, in 2001, and a full-time tenure Associate Professor, in 2005. His research interests are in the field of structure and control of power conditioning systems for autonomous systems, power factor correction, renewable energy applications, stability problems, nonlinear phenomena, bifurcations control. He was an Associate Editor of the *IET Circuits, Systems and Devices*, a Guest Editor of the IEEE JOURNAL ON EMERGING AND SELECTED TOPICS ON CIRCUITS AND SYSTEMS Special Issue on Design of Energy-Efficient Distributed Power Generation Systems, in 2015, a Guest Editor of the IEEE TRANSACTIONS ON CIRCUITS AND SYSTEMS—II, in 2018, and *Energies*, from 2018 to 2019. He currently serves as an Associate Editor for the *IET Power Electronics* and the *IET Electronics Letters*, an Associate Editor-in-Chief in the IEEE OPEN JOURNAL OF CIRCUITS AND SYSTEMS, and a Topic Editor in *Energies*.

ANGEL CID-PASTOR (Member, IEEE) graduated as Ingeniero Técnico Industrial en Electrònica Industrial and Ingeniero en Automàtica y Electrònica Industrial from Universitat Rovira i Virgili, Tarragona, Spain, in 1999 and 2002, respectively, the M.S. degree in design of microelectronics and microsystems circuits from the Institut National des Sciences Appliquées, Toulouse, France, in 2003, and the Ph.D. degree from Universitat Politècnica de Catalunya, Barcelona, Spain, and from the Institut National des Sciences Appliquées, LAAS-CNRS Toulouse, France, in 2005 and 2006, respectively. He is currently an Associated Professor with the Departament d'Enginyeria Electrònica, Elèctrica i Automàtica, Escola Tècnica Superior d'Enginyeria, Universitat Rovira i Virgili, Tarragona. He is a member of the Automatic Control and Industrial Electronics (GAEI) Research Group. His research interests are in the field of power electronics, power conditioning for electric vehicles, and renewable energy systems. He currently serves as a Subject Editor of Electronics Letters for *Power Electronics*.

ENRIC VIDAL-IDIARTE (Member, IEEE) received the Licenciado en Informatica and Ph.D. degrees from the UPC, Barcelona, Spain, in 1993 and 2001, respectively. He is currently an Associate Professor with the Departament d'Enginyeria Electrònica, Elèctrica i Automàtica, Universitat Rovira i Virgili, Tarragona, Spain, where he is working in the field of digital and robust control of power converters. He is a member of the Grup d'Automatica i Electròonica Industrial Research Group on Industrial Electronics and Automatic Control, whose main research fields are power conditioning for vehicles, satellites, and renewable energy.

HUGO VALDERRAMA-BLAVI (Member, IEEE) is currently an Associate Professor with the Department of Electronic Engineering and Automatic Control, Universitat Rovira i Virgili, Tarragona, Spain, where he is working in the field of power electronics for renewable energy and distributed generation systems, efficient lighting, high voltage gain conversion, and applications for silicon carbide devices.

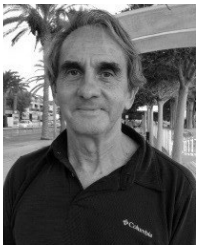

LUIS MARTINEZ-SALAMERO (Senior Member, IEEE) received the Ingeniero de Telecomunicación and Ph.D. degrees from the Universidad Politécnica de Cataluña, Barcelona, Spain, in 1978 and 1984, respectively.

From 1978 to 1992, he taught circuit theory, analog electronics, and power processing with the Escuela Técnica Superior de Ingenieros de Telecomunicación, Barcelona. From 1992 to 1993, he was a Visiting Professor with the Center for Solid State Power Conditioning and Control, Department of Electrical Engineering, Duke University, Durham, NC, USA. From 2003 to 2004, from 2010 to 2011, and from March 2018 to September 2018, he was a Visiting Scholar with the Laboratory of Architecture and Systems Analysis (LAAS), National Agency for Scientific Research (CNRS), Toulouse, France. Since 1995, he has been a Full Professor with the Department of Electrical Electronic and Automatic Control Engineering, School of Electrical and Computer Engineering, Rovira i Virgili University, Tarragona, where he managed the Research Group in Automatic Control and Industrial Electronics (GAEI), from 1998 to 2018. His research interests include structure and control of power conditioning systems, namely, electrical architecture of satellites and electric vehicles, as well as nonlinear control of converters and drives, and power conditioning for renewable energy.